Langmuir
Article
pubs.acs.org/Langmuir

Nanoparticle Charge Control in Nonpolar Liquids: Insights from Small-Angle Neutron Scattering and Microelectrophoresis

Roger Kemp,[†] Rodrigo Sanchez,[†] Kevin J. Mutch,[‡] and Paul Bartlett*[,†]

[†]*School of Chemistry, University of Bristol, Bristol BS8 1TS, United Kingdom and* [‡]*Condensed Matter Physics Laboratory, Heinrich-Heine-University, Düsseldorf, Germany*

Received November 5, 2009. Revised Manuscript Received December 27, 2009

Electrostatic forces are typically produced in low polarity solvents by the addition of surfactants or charge-control additives. Although widely used, there is no consensus on the mechanism by which surfactants control the level of particle charge. We report an investigation using highly sensitive, single particle optical microelectrophoresis measurements combined with a small-angle neutron scattering study to establish the mechanism of charging by the surfactant AOT in the nonpolar solvent *n*-dodecane. We show that polymer-grafted particles with no chemically bound surface charges only charge above the critical micellar concentration of the surfactant. The surface potential increases gradually with increasing surfactant concentration c, before finally saturating at high c. The increase in the surface potential is correlated to the amount of surfactant adsorbed onto the surface of the particle. Using deuterated AOT and contrast variation techniques, we demonstrate that the surfactant is adsorbed within the polymer layer surrounding the particle core, probably as individual molecules rather than surfactant aggregates. A simple thermodynamic model accounts for the concentration dependence of the observed surface potential.

1. Introduction

The response of colloids and nanoparticles to external electric fields has proved to be an extremely flexible and powerful technique to control the self-assembly of functional materials. Field-responsive photonic structures form the basis for a wide range of current and future technologies with applications in areas such as full-color display units,[1,2] flexible electronic replacements for paper,[3−5] chemical and biochemical sensors,[6] data storage media, and active optical components.[7] Such practical applications often require the use of organic solvents for ease of fabrication or for long-term stability. However, while colloidal and nanoparticle dispersions are often highly charged in water, it is much more challenging to generate charge in organic, nonpolar solvents ("oils"). The reason is simply the low dielectric constant of an oil (typically ∼2) which ensures that the energy barrier to charge separation in an oil is about 40 times larger than that in water. Charged particles, although rare in nonpolar solvents, are not unknown with the earliest experimental demonstration of particle charging, dating back at least to the 1950s. More recent experiments, using the surface force apparatus,[8,9] atomic force microscope, and optical tweezers,[10] have clearly confirmed the existence of long-range repulsive electrostatic interactions between particles and surfaces in nonpolar solvents. The issue of charge control in oils has become more topical recently because of the intense drive to develop thin, lightweight, and ultimately paperlike displays based on electrophoretic technologies.

Typically, in the majority of these examples, nonpolar dispersions are charged by the addition of, what are termed euphemistically, "charge-control additives" (CCAs). Although the exact details are not always clear, it is generally assumed[11] that CCAs function as surfactants in the organic, nonpolar solvents used and form reversed micelles. The CCA has probably two distinct roles in these systems. First, it forms micelles with an inverse structure consisting of a hydrophilic core, surrounded by the hydrophobic portions of the amphiphile. The reversed micelles encapsulate and stabilize any counterions in solution by forming, in effect, a dressed, sterically stabilized "nanoion". This has the effect of reducing the energy barrier for charge separation. Second, the added surfactant may adsorb onto the surface of the particle and dissociate to generate additional charged surface groups on the particle. Although the central role of reversed micelles has been emphasized by Hsu et al,[12] the exact chemical mechanism of particle charging in nonpolar solvents remains uncertain and vague.

In this Article, we present a combined study of the adsorption and charging generated by the surfactant aerosol-OT (AOT, or sodium di-2-ethylhexylsulfosuccinate) on a sterically stabilized nanoparticle which has no chemically bound surface charges in *n*-dodecane.The structure of the adsorbed surfactant layer on the grafted composite particle is determined by small-angle neutron scattering (SANS), using contrast variation techniques. Previous investigations have demonstrated that SANS is highly suited to elucidate the radial structure of composite latex particles. In particular, if the contrast of the particles against the surrounding medium is low, the process of adsorption of polymers or surfactants with high scattering length density onto these particles may be studied readily by SANS. In our experiments the contrast of an

*To whom correspondence should be addressed. E-mail: p.bartlett@bristol.ac.uk. Telephone: +44 (0)117 9546880. Fax: +44 (0)117 9250612.

(1) Arsenault, A. C.; Puzzo, D. P.; Manners, I.; Ozin, G. A. *Nat. Photonics* **2007**, *1*, 468–472.
(2) Fudouzi, H.; Xia, Y. N. *Langmuir* **2003**, *19*, 9653–9660.
(3) Comiskey, B.; Albert, J. D.; Yoshizawa, H.; Jacobson, J. *Nature* **1998**, *394*, 253–255.
(4) Chen, Y.; Au, J.; Kazlas, P.; Ritenour, A.; Gates, H.; McCreary, M. *Nature* **2003**, *423*, 136–136.
(5) Sikharulidze, D. *Appl. Phys. Lett.* **2005**, *86*, 033507.
(6) Holtz, J. H.; Asher, S. A. *Nature* **1997**, *389*, 829–832.
(7) Cho, S. N. *J. Appl. Phys.* **2009**, *106*, 033505.
(8) Briscoe, W. H.; Horn, R. G. *Langmuir* **2002**, *18*, 3945–3956.
(9) McNamee, C. E.; Tsujii, Y.; Matsumoto, M. *Langmuir* **2004**, *20*, 1791–1798.
(10) Sainis, S. K.; Merrill, J. W.; Dufresne, E. R. *Langmuir* **2008**, *24*, 13334–13347.
(11) Morrison, I. D. *Colloids Surf.* **1993**, *71*, 1–37.
(12) Hsu, M. F.; Dufresne, E. R.; Weitz, D. A. *Langmuir* **2005**, *21*, 4881–4887.

isotopic mixture of h_{26}-dodecane and d_{26}-dodecane is varied to match the average scattering density of the nanoparticle so that the observed scattering $I(q)$ ($q=(4\pi/\lambda)\sin(\theta/2)$; θ, scattering angle and λ, wavelength) derives predominately from the adsorbed layer of surfactant.

2. Scattering Theory

We consider the scattering by a surfactant adsorbed onto a dilute dispersion of colloidal particles, in the presence of excess micelles. We assume, first, that the colloidal particles have a radially symmetric core−shell structure consisting of a solid core surrounded by an outer polymer shell and, second, that the dispersion is sufficiently dilute that the particles are noninteracting and the structure factor $S(q) = 1$. For such spherically symmetric particles, the intensity of scattered radiation is equal to $b(q)^2$, where the scattering amplitude $b(q)$ is given by the well-known expression

$$b(q) = 4\pi \int_0^\infty r^2 \, \mathrm{d}r \frac{\sin qr}{qr}[\rho(r) - \rho_\mathrm{m}] \tag{1}$$

Here, $\rho(r)$ is the radial scattering length density profile and ρ_m is the scattering length density of the suspension medium.

In our experiments, the surfactant is characterized by a scattering length density large by comparison to either that of the core of the particle or that of the surrounding polymer shell. As we show later, the surfactant adsorbs into the shell of the particle so the amplitude of scattering from the particle depends sensitively on the amount of surfactant adsorbed. To recognize this dependency, we write the scattering length density profile of the surfactant-coated particle, at a surfactant concentration c, as

$$\rho(r) = \rho_\mathrm{P}(r) + \delta\rho_\mathrm{S}(r) \tag{2}$$

where $\rho_\mathrm{P}(r)$ is the scattering profile of the particle before adsorption and $\delta\rho_\mathrm{S}(r)$ is the change in the scattering profile produced by the adsorption of surfactant into the shell of the particle. Figure 1 gives a pictorial representation of this model.

The total intensity $I(q,c)$ scattered per unit sample volume by a suspension of noninteracting surfactant-coated particles and micelles at a surfactant concentration of c may be written as the sum of four terms:

$$I(q,c) = \bar{I}_\mathrm{PS}(q,c) + I_\mathrm{M}(q,c) + \tilde{I}_\mathrm{P}(q) + \tilde{I}_\mathrm{S}(q,c) \tag{3}$$

The first term $\bar{I}_\mathrm{PS}(q,c)$ in eq 3 details the scattering of a uniform surfactant-coated particle. In the case discussed here, the core and shell, before surfactant adsorption, have a low excess scattering length density. In contrast, the surfactant has a high excess scattering length density so $\bar{I}_\mathrm{PS}(q,c)$ is dominated by the contribution from the surfactant. The second term, $I_\mathrm{M}(q,c)$, is simply the scattering from free micelles in solution, whereas $\tilde{I}_\mathrm{P}(q)$ and $\tilde{I}_\mathrm{S}(q,c)$ refer to the scattering produced by the density fluctuations in the particle before adsorption and in the shell of the surfactant-coated particle, respectively. The term $\tilde{I}_\mathrm{P}(q)$ takes into account explicitly the fluctuations, $\rho_\mathrm{P}(r) - \langle\rho_\mathrm{P}(r)\rangle$, of the scattering profile from the average for the particle in the absence of surfactant, while $\tilde{I}_\mathrm{S}(q,c)$ is the analogous contribution from thermal density fluctuations within the shell of the surfactant-coated particle. Both terms vanish for homogeneous density profiles and have been analyzed by Auroy, Auvray, and co-workers[13−15] in the situation of adsorbed polymer layers. For the thin surfactant layers investigated in this study, the thermal fluctuations which contribute to $\tilde{I}_\mathrm{S}(q,c)$ are expected to be negligible in the q-range employed here. Hence, we will from here onward ignore this term in our discussion.

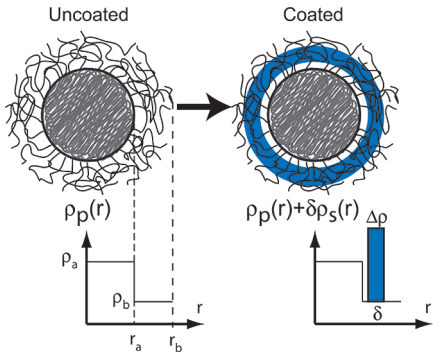

Figure 1. Sketch of the process of adsorption of a surfactant (shown in blue) onto a polymer grafted nanoparticle and the resulting change in the scattering length density profile. The scattering length density of the core is ρ_a, the polymer layer is ρ_b, and the adsorbed surfactant is modeled by a homogeneous band of thickness δ_S and scattering density $\Delta\rho$.

To analyze the data, we recall that the intensity scattered by the particles in the absence of surfactant is

$$I(q,0) = \bar{I}_\mathrm{PS}(q,0) + \tilde{I}_\mathrm{P}(q) \tag{4}$$

so that the change in the scattered intensity, $\Delta I(q,c) = I(q,c) - I(q,0)$, produced by adding different concentrations c of the surfactant is from eq 3,

$$\begin{aligned}\Delta I(q,c) &= [\bar{I}_\mathrm{PS}(q,c) - \bar{I}_\mathrm{PS}(q,0)] + I_\mathrm{M}(q,c) \\ &= \Delta\bar{I}_\mathrm{PS}(q,c) + I_\mathrm{M}(q,c)\end{aligned} \tag{5}$$

The characteristic length scale R_g of the micelles is of order of a few nanometers (cf. section 4.5), whereas the diameter of the particles used is of order 100 nm. Since the scattering from the micelles at $q = 0$ scales with R_g^3, the scattering from the particles dominates at small q. As a consequence, $\Delta I(q,c)$ measured up to $q \sim 10^{-2}$ Å^{-1} is well approximated solely by $\Delta\bar{I}_\mathrm{PS}(q,c)$. At high q, the particle scattering decreases as q^{-4} (Porod law) so that $I_\mathrm{M}(q,c)$ becomes the dominant term at high scattering angles. The leading contribution to the difference intensity at small q is the change in particle scattering caused by surfactant adsorption, $\Delta\bar{I}_\mathrm{PS}(q,c)$. In the noninteracting dilute limit where $S(q) = 1$, this may be expressed as

$$\Delta\bar{I}_\mathrm{PS}(q,c) = n_\mathrm{P}\left[2b_\mathrm{P}(q)\delta b_\mathrm{S}(q) + \delta b_\mathrm{S}(q)^2\right] \tag{6}$$

where n_P is the number density of colloidal particles, b_P is the amplitude of scattering from a particle in the absence of added surfactant, and δb_S is the *change* in the scattering amplitude of the shell of the particle generated by surfactant adsorption

$$\delta b_\mathrm{S}(q) = 4\pi \int_0^\infty r^2 \, \mathrm{d}r \frac{\sin qr}{qr}\delta\rho_\mathrm{S}(r) \tag{7}$$

In the experiments detailed below, we use mixtures of protonated and deuterated solvents to minimize the scattering intensity from the uncoated particle so that the scattering signal is due predominantly to the adsorbed surfactant. In the immediate neighborhood of the (average) contrast match point of the particle,

(13) Auroy, P.; Auvray, L.; Leger, L. *Macromolecules* **1991**, *24*, 2523–2528.
(14) Auvray, L.; Cotton, J. P. *Macromolecules* **1987**, *20*, 202–207.
(15) Auvray, L.; de Gennes, P. G. *Europhys. Lett.* **1986**, *2*, 647–650.

Table 1. Reagent Masses and Solvents Used in Dispersion Polymerization of Latices RK2 and AC2

batch	$\langle R_p \rangle$ (nm)	MMA (g)	MAA (g)	PHS-*g*-PMMA (g)	hexane (g)	*n*-dodecane (g)	octanethiol (g)	AIBN (g)
RK2	46	21.0	0.43	14.3	25.6	3.0	0.11	0.26
AC2	425	33.1	0.68	5.3	19.4	6.0	0.17	0.26

where $b_P(q=0)=0$, we expect $b_P(q)$ to be small and negligible in comparison to $\delta b_S(q)$. For a uniform particle, the scattering is exactly zero at all wavevectors at the contrast match point. However, this statement is no longer in general true for a core−shell particle where interference between the amplitudes scattered by the core and shell generates finite scattering at nonzero q even when the intensity at $q=0$ is zero. The core−shell particles used in this study are however rather propitious. Contrast-variation measurements (cf. section 4.4) reveal that these particles are remarkably homogeneous with a small contrast difference between the core and shell, in the absence of surfactant. Consequently, in the present case, we may safely write $\Delta\bar{I}_{PS}(q,c) \approx n_P[\delta b_S(q)]^2$ since the scattering is dominated by the change in scattering amplitude of the particle shell produced by surfactant adsorption.

For simplicity, we assume that the surfactant is adsorbed in a uniform band of inner radius a_S and thickness δ_S so that the scattering length density of the particle, after surfactant adsorption, becomes $\rho_P(r) + \delta\rho_S(r)$ where

$$\delta\rho_S(r) = \begin{cases} 0 & \text{if} \quad r < a_S \\ \Delta\rho & \text{if} \quad a_S \le r \le a_S + \delta_S \\ 0 & \text{if} \quad r > a_S + \delta_S \end{cases} \tag{8}$$

Here, $\Delta\rho$ is the scattering length density of the uniform band of adsorbed surfactant. The change in the amplitude of scattering from the shell of the particle produced by surfactant adsorption is therefore

$$\delta b_S(q) = 4\pi {a_S}^3 \Delta\rho \left[{\lambda_S}^2 \frac{j_1(q\lambda_S a_S)}{qa_S} - \frac{j_1(qa_S)}{qa_S} \right] \tag{9}$$

where $\lambda_S = 1 + \delta_S/a_S$ and $j_1(x) = (\sin x - x\cos x)/x^2$ is the first-order spherical Bessel function.

3. Experimental Section

3.1. Materials. All solvents were analytical grade and used as received. Unless indicated otherwise, we used dried *n*-dodecane for our experiments. The progress of drying was monitored by conductivity; a specific conductivity of ≤ 5 fS cm^{-1} was judged to be sufficiently low compared with the conductivity of the AOT solutions as to be neglected. The monomers methyl methacrylate (MMA) and the methacrylic acid (MAA) were obtained from Sigma-Aldrich and stored at 5 °C. Immediately prior to use, the inhibitor was removed by passing the monomer through a disposable silica-gel column (Sigma-Aldrich). The initiator azobisisobutyronitrile AIBN (Sigma-Aldrich) and chain transfer agent octanethiol (Sigma-Aldrich) were used as received. The PHS-*g*-PMMA comb stabilizer was synthesized following the procedure outlined by Antl et al.[16] The hydrogenated surfactant Aerosol OT (*h*-AOT, or sodium di-2-ethylhexylsulfosuccinate) was purchased from Fluka BioChemika (<99% purity). It was purified by Soxhlet extraction with ethyl acetate. The ethyl acetate was removed by rotary evaporation, and the AOT dried in a vacuum oven. The surfactant was then dissolved in distilled methanol and centrifuged for 30 min at 3800 rpm to remove any remaining inorganic impurities. Finally, the methanol was removed by rotary evaporation, and the AOT was dried in a vacuum oven. The purified surfactant was stored in a desiccator prior to use. Deuterated 2-ethyl hexanol was obtained from the Oxford Isotope Facility (Oxford, U.K.), and d_{26}-dodecane was purchased from Sigma-Aldrich.

3.2. Particles. In all experiments, we used hydrogenated poly(methyl methacrylate) (PMMA) particles sterically stabilized by a thin covalently attached layer of poly(12-hydroxy stearic) acid (PHS). The PHS is fixed on the surface of the particle. Electrophoretic measurements[17] showed that when dispersed in low polarity solvents the particles have no chemically bound surface charges and are stabilized solely by polymeric forces. The PMMA spheres were prepared in a dispersion polymerization by copolymerizing methyl methacrylate, methacrylic acid, and a PHS-*g*-PMMA macromonomer.[16] Two latex formulations with different mean radii were synthesized. The system of small particles is labeled here as RK2 and the larger spheres as AC2. The amounts of reactants and solvents used in each synthesis are listed in Table 1. After synthesis, the latices were purified by repeated washing and centrifugation in *n*-dodecane to remove any unreacted species. The process was repeated at least five times to ensure complete solvent exchange before the particles were suspended in dried *n*-dodecane and stored under nitrogen.

Dilute dispersions of the large AC2 particles were deposited on glass coverslips attached to aluminum planchettes, dried, and sputter coated with gold before being imaged using a JEOL JSM-6310 scanning electron microscope. Analysis of approximately 1000 particles yielded a number average particle radius of $\langle R_p \rangle = 425 \pm 25$ nm and a polydispersity of $\varepsilon_p = 0.10 \pm 0.01 (\varepsilon_p{}^2 = \langle \delta R_p{}^2 \rangle / \langle R_p \rangle^2)$. Dilute dispersions of the small RK2 latices in *n*-dodecane were characterized by dynamic light scattering at a wavelength of 532 nm, using a Malvern 4700 autosizer (Malvern, U.K.). A mean hydrodynamic radius R_h of 51.8 ± 0.2 nm was extracted from a third-order cumulant fit to the intensity autocorrelation function $g_2(\tau)$, measured at 16 equally spaced scattering angles between 70 and 120°.

3.3. Deuterated Surfactant. Partially deuterated AOT (d_{34}-AOT) was prepared by diesterification of hydrogenated maleic anhydride with deuterated 2-ethyl hexanol. The deuterated alcohol, maleic anhydride (Avocado, 99%), and toluene-4-sulfonic acid monohydrate (Aldrich, 98.5%) were reacted in toluene, using a Dean and Stark trap to remove water. The mixture was refluxed with stirring for approximately 6 h. When the volume of water evolved from the reaction was comparable with the theoretical maximum, the mixture was cooled to 70 °C and washed with hot water to remove unreacted maleic anhydride and sulfonic acid. The crude diester was obtained by rotary evaporation and purified by washing through a silica column with a 7% mixture of diethyl ether and 60:40 petroleum ether. The purified diester was sulfonated in a 2:1 solvent mixture of ethanol/water by reflux with an excess amount of sodium sulfite and sodium metabisulfite (both Avocado, 97%). Thin layer chromatography was used to check for disappearance of the high-running diester spot. The crude surfactant was separated by rotary evaporation and purified by Soxhlet extraction with ethyl acetate. After removal of the solvent and drying in a vacuum oven, centrifugation in distilled methanol for 30 min at 3800 rpm was used to remove any remaining inorganic impurities. This process was repeated until no further salts remained. The crude and cleaned diester, and the final product were analyzed by ^{1}H, ^{2}H, and ^{13}C NMR. The final deuterated surfactant contains three residual hydrogen atoms in

(16) Antl, L.; Goodwin, J. W.; Hill, R. D.; Ottewill, R. H.; Owens, S. M.; Papworth, S.; Waters, J. A. *Colloids Surf.* **1986**, *17*, 67–78.

(17) Roberts, G. S.; Sanchez, R.; Kemp, R.; Wood, T.; Bartlett, P. *Langmuir* **2008**, *24*, 6530–6541.

the headgroup (due to the use of hydrogenated maleic anhydride), giving the chemical formula $Na^+-C_{20}D_{34}H_3O_7S^-$. Assuming the molar volume is 649 Å^3, as measured for *h*-AOT in *p*-xylene,[18] we estimate a coherent scattering length density of 6.08×10^{-6} Å^{-2}.

3.4. Electrical Conductivity Measurements. The conductivity of *h*-AOT solutions in dried *n*-dodecane were measured using a model 627 conductivity meter (Scientifica, Princeton, NJ). The instrument consisted of a stainless steel cup probe that was fully immersed in a 2 mL sample. The ionic strength and Debye screening length κ^{-1} of the solution were calculated from a knowledge of the micellar radius and the solvent viscosity.

3.5. Adsorption Isotherm. Different amounts of *h*-AOT with concentrations between 0 and 10 mol m^{-3} were added to dispersions of PMMA particles in *n*-dodecane ($\varphi_c = 0.1$) with a mean radius of $\langle R_p \rangle = 46$ nm. The mixture was equilibrated at 20 °C for 48 h before being centrifuged at 10 000 rpm for 6 h to separate the particles from the supernatant. The equilibrium concentration of surfactant in the supernatant was determined by Fourier transform infrared (FT-IR) adsorption using the broad peak at 1738 cm^{-1} which corresponds to the carbonyl stretch of the two C═O bonds in the AOT molecule. Calibration experiments confirmed that the recorded absorbance was linear in the concentration of AOT. The quantity of AOT adsorbed on the particles was then deduced by mass balance.

3.6. Electrophoretic Mobility Measurements. The particle charge was quantified by means of single particle optical microelectrophoresis (SPOM) measurements on very dilute suspensions ($\varphi_c \sim 1 \times 10^{-5}$) of AOT in *n*-dodecane using the procedure developed by Roberts et al.[19] Typically, 50 statistically different individual particles were measured at each surfactant concentration, and the mean mobility and standard deviation were recorded. The standard electrokinetic model of O'Brien and White[20] was used to convert the measured mobilities into equivalent zeta potentials using the measured Debye screening length and estimates of the limiting micellar conductances.

3.7. SANS Experiments. SANS measurements were performed on the recently refurbished D11 small-angle diffractometer at the Institute Laue Langevin (Grenoble, France). The instrument has a 2D area detector consisting of 128 × 128 cells, each 7.5 mm square. Measurements were made at three sample−detector distances (1.2, 6, and 39 m) and two collimation lengths (8 and 40.5 m) at $\lambda = 6$ Å to give a *q*-range of $3 \times 10^{-3} < q < 0.5$ Å^{-1}. All of the samples were contained in 1 mm path length rectangular quartz cells and recorded at 25 °C. Two-dimensional spectra were azimuthally averaged and corrected for background electronic noise, cell scattering, and finite transmission using standard programs. The raw intensity data were converted into absolute units using the incoherent scattering recorded from a sample of water. For the particle concentration ($\varphi_c = 0.02$) used here, the structure factor $S(q)$ differs from unity only in a *q*-range smaller than 0.002 Å^{-1}. For higher *q* values, $S(q) \approx 1$ within experimental errors, and consequently, the influence of interparticle correlations may be safely ignored.

4. Results and Discussion

4.1. Reversed Micelle Formation. Many studies have confirmed that the double-tailed anionic surfactant AOT readily forms spherical reversed micellar structures that encapsulate pools of water when dissolved in apolar solvents such as *n*-dodecane. Small-angle X-ray and neutron measurements reveal that the size of the water pool may be tuned by changing the molar ratio of water to surfactant, while the measured critical micellar concentration (CMC) depends decisively on the exact amount of water present in the system.[21] Experimentally, since the surfactant cannot be fully desiccated without partly decomposing it, AOT solutions prepared from even nominally dry solvents always contain trace quantities of water. As water markedly increases the tendency to aggregate, there is considerable uncertainty in the literature over the exact value of the CMC for AOT in nonpolar solvents or even if a viable CMC exists at all. To avoid this uncertainty, we characterized all surfactant solutions immediately prior to their use by conductivity. We observed a broad but marked change in the conductivity of solutions in dry *n*-dodecane with increasing AOT concentration which we identify as a critical concentration below which no micelle formation occurs.

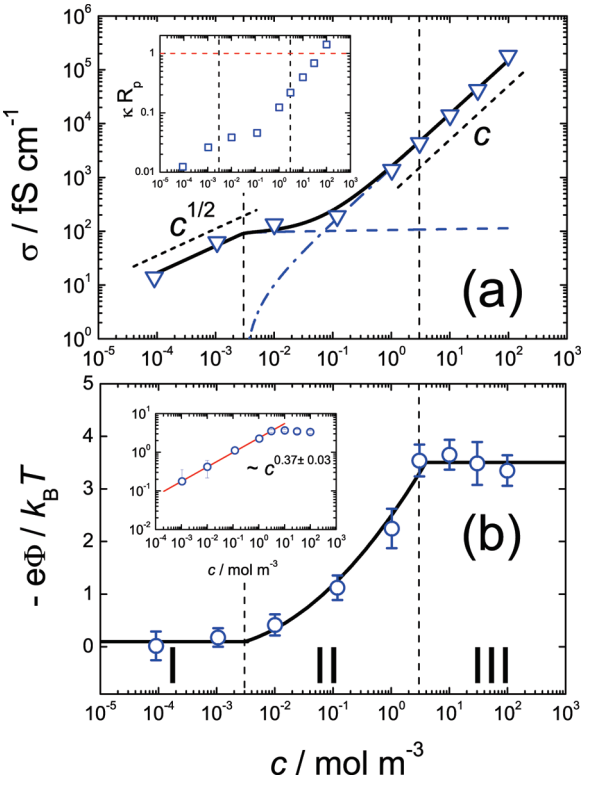

Figure 2. (a) Conductivity of AOT/*n*-dodecane solutions without added particles as a function of AOT concentration. The symbols indicate measurements, and the solid line is a fit to eq 11 with a CMC of 3×10^{-3} mol m^{-3}. The dashed and dotted lines are the contributions to the total conductivity from the dissociation of monomers and the thermal ionization of micelles, respectively. The inset shows the equivalent values of κR_p, estimated for the AC2 particles. Note that all measurements lie in the low-κR_p regime ($\kappa R_p < 1$) except for the most concentrated sample in region III where $\kappa R_p = 1.4$. (b) Dimensionless surface potential, determined from electrophoretic mobility measurements, of AC2 particles in *n*-dodecane as a function of the AOT concentration *c*. The inset shows that in region II the surface potential grows approximately as $c^{0.4}$.

The conductivity σ of micellar solutions of AOT in *n*-dodecane as a function of the weighed-in concentration of the surfactant *c* is displayed in Figure 2a. Following Sainis et al.,[10] we divide the graph into three distinct regions. At very low AOT concentrations (region I), the conductivity initially scales like $\sigma \propto \sqrt{c}$ and then grows smoothly and nonlinearly in an intermediate rather broad range of concentrations (region II), before ultimately displaying a linear dependence, $\sigma \propto c$, at high surfactant concentrations (region III). In region I, the square-root dependence is consistent

(18) Ekwall, P.; Mandell, L.; Fontell, K. *J. Colloid Interface Sci.* **1970**, *33*, 215.
(19) Roberts, G. S.; Wood, T. A.; Frith, W. J.; Bartlett, P. *J. Chem. Phys.* **2007**, *126*, 194503.
(20) O'Brien, R. W.; White, L. R. *J. Chem. Soc., Faraday Trans. II* **1978**, *74*, 1607–1626.
(21) Eicke, H. F.; Christen, H. *Helv. Chim. Acta* **1978**, *61*, 2258–2263.

with the dissociation of monomeric surfactant molecules, that is, $Na-AOT \overset{K_S}{\rightleftharpoons} Na^+ + AOT^-$, since applying the law of mass action we expect $[Na^+] = [AOT^-] = K_S^{1/2}\sqrt{c}$, if we neglect the small number of ions. At high surfactant concentrations (region III), above the CMC, the linear increase of the conductivity σ seen with c is consistent with the charge fluctuation model proposed by Eicke and co-workers[22−24] for micelles. Charge separation is generated by a statistical fluctuation, in which an ion transfers between two colliding neutral surfactant micelles (M) to produce, on separation, two oppositely charged micelles $M + M \overset{K_M}{\rightleftharpoons} M^+ + M^-$, with K_M being the equilibrium constant for micelle charging. Since the solution must remain electrically neutral, we get under the condition $c \gg c_{cmc}$ (c_{cmc} is the surfactant concentration at the CMC),

$$[M^+] = [M^-] = {K_M}^{1/2}[M] \sim \frac{{K_M}^{1/2}}{\langle N_{as}\rangle}\, c \qquad (10)$$

where $\langle N_{as}\rangle$ is the mean association number of the micelles. In the vicinity of the CMC (region II), both ionization of monomers and thermal charging of micelles contribute to the measured conductivity. The conductivity σ of a dilute electrolyte solution of different ions i with valency z_i and number density ρ_i is $\sigma = e^2\Sigma_i {z_i}^2(\rho_i/\xi_i)$ where the friction coefficient ξ_i is $6\pi\eta r_i$, η is the viscosity of the solvent, and r_i is the radius of the ith ionic species. The conductivity of a mixture of monomeric surfactant molecules (S) and micelles (M) may therefore be written as

$$\sigma = N_A e^2 \left[\left(\frac{1}{\xi_+} + \frac{1}{\xi_-} \right) \sqrt{K_S}[S]^{1/2} + \frac{2}{\xi_M} \sqrt{K_M}[M] \right] \qquad (11)$$

where ξ_+, ξ_-, and ξ_M are the friction coefficients, respectively, of the Na^+, AOT^-, and micellar species. The concentration of free surfactant [S] and micelles [M] changes rapidly with the weighed − insurfactant concentrations c in the vicinity of the CMC. To calculate [S] and [M] as a function of c we model micellization with the closed − association model.[25] We assume the micelles have a fixed association number N_{as}, so that the solution contains only monomers and micelles, that is $N_{as}S \overset{K_N}{\rightleftharpoons} M$ with K_N being the equilibrium constant for micelle formation. The total surfactant concentration in the system c is then simply $c = N_{as}K_N[S]^{N_{as}} + [S]$ which for a given K_N is readily solved at each c to give the free surfactant concentration [S] and the corresponding micelle concentration ($[M] = K_N[S]^{N_{as}}$). For sufficiently large association numbers N_{as}, the fraction of the added surfactant which goes into the micelle, $d\{N_{as}[M]\}/dc$, increases sharply with total surfactant concentration c. We identify the CMC as the concentration point where an added monomer is equally likely to enter a micelle as to remain in solution, that is, $dN_{as}[M]/dc = 0.5$ which yields the expression,[25]

$$CMC = \left(1 + \frac{1}{N_{as}}\right)\left({N_{as}}^2 K_N\right)^{-1/(N_{as}-1)} \qquad (12)$$

A fit of the conductivity measured for AOT in dry *n*-dodecane to eq 11 is shown by the solid line in Figure 2a. Using the association number $N_{as} = 28$ obtained from ultracentrifugation measurements by Peri,[26] we obtain a CMC of 3×10^{-3} mol m^{-3}. This value is comparable to estimates obtained previously by both Sainis et al.[10] for AOT in dry hexadecane and by Eicke and Arnold[27] in carefully dried benzene.

4.2. Nonpolar Particle Charging. Electrophoretic mobility measurements suggest that our particles develop large surface potentials in the presence of AOT reverse micelles. To quantify particle charging, we used single particle optical microelectophoresis[19] to probe the dimensionless surface potential $e\Phi/k_BT$ produced on large $\langle R_p\rangle = 425$ nm PMMA particles by the addition of *h*-AOT. Due to the method of synthesis, the particles bear no chemically bound charges and are stabilized solely by a thin (∼10 nm) covalently grafted layer of poly(12-hydroxystearic acid). To elucidate the role of reverse micelles in particle charging we have exploited the sensitivity of the SPOM technique to determine the particle surface potential over a wider range of surfactant concentrations (from 10^{-4} to 10^2 mol m^{-3}) than previously reported.[17] The variation of the surface potential $e\Phi/k_BT$ with surfactant concentration c is plotted in Figure 2b. We divide the response into three regimes. In region I, where reverse micelles are not present ($c < 3 \times 10^{-3}$ mol m^{-3}), the particles exhibit no net response to an electric field, consistent with a lack of ionizable groups on the surface of the particle. The average charge $\langle Z\rangle$ (in units of the fundamental charge e) measured on 80 particles is essentially indistinguishable from zero, $\langle Z\rangle = -1.2 \pm 2.6$. The particles first charge in concentration region II ($3 \times 10^{-3} < c < 3$ mol m^{-3}). Here, above the CMC, a finite surface potential appears which becomes progressively more negative as the concentration of AOT is increased. This observation suggests that reverse micelles play a central role in the mechanism of particle charging. The particles develop a finite potential only as reverse micelles appear and φ grows as the concentration of reverse micelles grows for $c > c_{cmc}$. We can get further insights into the role of reverse micelles by a quantitative analysis of the charging data. The inset to Figure 2b reveals that the particle potential in regime II grows surprisingly slowly with added surfactant. Indeed, Φ appears to display a weak power-law dependence on the growing concentration of micelles above the CMC with $|\Phi| \propto c^{0.37\pm0.03}$. The observation that Φ increases sublinearly with increasing surfactant concentration is inconsistent with the recent suggestion[17] that particles charge by surface adsorption of reverse micelles. In this mechanism, the particle potential should be, at least initially, proportional to the number of micelles adsorbed. Since the number adsorbed will depend linearly on the micelle concentration in solution which, above the CMC, will be proportional to the added surfactant concentration c, we expect a limiting linear dependence, $|\Phi| \propto c$. We will return in section 4.7 to reexamine the mechanism of particle charging in nonpolar solvents and propose a new mechanism which is consistent with the observations presented in this paper. Finally, at the highest surfactant concentrations (region III: $c > 3$ mol m^{-3}), Figure 2b reveals that the concentration dependence of Φ changes significantly. In agreement with earlier measurements,[12,17] we observe that at high surfactant concentrations the surface potential is essentially independent of c. We find a plateau potential of $e\Phi/k_BT = -3.5 \pm 0.1$ which is in good agreement with measurements previously reported.[10,17] For the SANS measurements reported in section 4.6, we used small PMMA particles with a mean radius of $\langle R_p\rangle = 46$ nm in contrast to the larger PMMA spheres ($\langle R_p\rangle = 425$ nm) studied in the SPOM measurements above. Although the 46 nm particles are too small

(22) Eicke, H. F.; Borkovec, M.; Das-Gupta, B. *J. Phys. Chem.* **1989**, *93*, 314–317.
(23) Kallay, N.; Chittofrati, A. *J. Phys. Chem.* **1990**, *94*, 4755–4756.
(24) Hall, D. G. *J. Phys. Chem.* **1990**, *94*, 429–430.
(25) Evans, D. F.; Wennerstrom, H. *The Colloidal Domain: Where Physics, Chemistry, Biology and Technology Meet*, 2nd ed.; Wiley: New York, 1999.
(26) Peri, J. B. *J. Colloid Interface Sci.* **1969**, *29*, 6–15.
(27) Eicke, H.; Arnold, V. *J. Colloid Interface Sci.* **1974**, *46*, 101–110.

to be studied by SPOM methods, we checked that the small PMMA particles behaved similarly to the larger PMMA system by measuring their surface potential in the high surfactant concentration regime. Electrophoretic mobilities were measured by phase analysis light scattering (Zetasizer Nano, Malvern, U.K.) at particle volume fractions $\varphi_c \sim 4 \times 10^{-5}$ and AOT concentrations between 3 and 4 mol m^{-3}. The mobilities equate to a surface potential of $e\Phi/k_BT = -2.8 \pm 0.7$ which given the difficulties of measuring the mobilities of these small particles (reflected in the large error limits) are comparable with the values obtained on the larger $\langle R_p \rangle = 425$ nm PMMA particles. Although the relative insensitivity of phase analysis light scattering prevented us from determining the full concentration dependence of the surface potential in the 46 nm system, the similarity in the plateau surface potential to the value obtained from the larger 425 nm particles, despite almost an order of magnitude difference in size, suggests that the charging behavior is probably size independent or at least relatively insensitive to the size of the particle. This suggestion is supported by previous observations on the same system.[17]

4.3. Surfactant Adsorption. It is well-known that adding AOT reverse micelles to a nonpolar colloidal suspension dramatically increases the particle charge.[12] However, the precise mechanism of colloid charging remains unknown and contentious. Morrison in an extensive review[11] proposed three plausible mechanisms to account for particle charging: (I) dissociation of surface groups, (II) preferential adsorption of charged hydrophobic species only (either ions or micelles), or (III) adsorption of neutral species followed by ion exchange with surface groups and the subsequent desorption of mobile ions so that the surface contained both neutral and charged species. The observation (in section 4.2) that, below the CMC, our particles are uncharged suggests that dissociation of surface groups (mechanism (I)) is probably unimportant but to emphasize that either mechanism II or III is operating we have confirmed that the appearance of a finite particle charge correlates with the adsorption of a surfactant species.

The experimentally determined adsorption isotherm of AOT onto the small ($\langle R_p \rangle = 46$ nm) PMMA spheres is reproduced in Figure 3a. The quantity of adsorbed surfactant Γ, experimentally measured as the mass of AOT adsorbed per unit mass of PMMA, is converted to μmol m^{-2} of AOT using the known surface area of the PMMA particles and the molar mass of AOT. The shape of the isotherm is well reproduced by a Langmuir function (solid line in Figure 3a), suggesting a high affinity adsorption process and a finite limit of adsorption. At high surfactant concentrations, the plateau value of about 0.6 μmol m^{-2} is reached at $c = 3$ mol m^{-3}. This corresponds to a relatively high surface area per dry AOT molecule of 260 Å^2. For comparison the area occupied per AOT molecule at the oil−water interface is significantly smaller, typically about 63 Å^2.[28,29] The large area per molecule measured at the PMMA surface indicates that the surfactant layer on the particle is not homogeneous but we will postpone a detailed discussion of the consequences of the area per molecule for the geometry of adsorption until after the structural data has been presented in section 4.6. The second interesting observation is the striking similarity between the adsorption isotherm and the particle charging behavior evident in a comparison of Figure 3a and b. The fact that both curves show a very similar increase with increasing surfactant concentration supports the notion that particle charging occurs either by surface adsorption of ionic species (mechanism II) or via the adsorption of neutral surfactant molecules, micelles, or hemimicelles and their subsequent ionization (mechanism III).

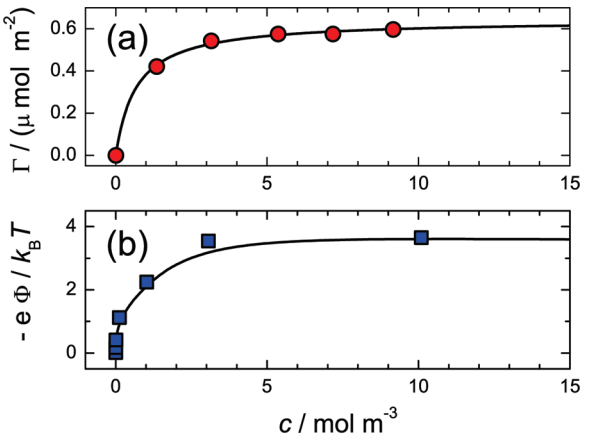

Figure 3. (a) Adsorption isotherm of AOT from *n*-dodecane onto particle RK2 (circles). The fitted Langmuir isotherm is shown as the solid line. (b) Surface potential of particle AC2 as a function of added AOT.

4.4. Scattering from Particles. To elucidate the identity and structure of the adsorbed species, we have conducted a small-angle neutron scattering study on mixtures of small $\langle R_p \rangle = 46$ nm PMMA spheres and AOT reverse micelles in *n*-dodecane. To enhance the scattering from the adsorbed surfactant and so focus on the structure of the adsorbed layer, we utilized deuterated surfactant (d_{34}-AOT) in combination with protonated particles (*h*-PMMA). The particle scattering was reduced, which would otherwise overwhelm the scattering from the considerably smaller surfactant micelles (R_m = 1.5 nm), by using contrast variation techniques and working near to the volume averaged contrast match point of the protonated particles. The PMMA particles were dispersed in a solvent mixture of h_{26}-dodecane and d_{26}-dodecane.

We first determine the volume averaged scattering length density, $\overline{\rho}_P = V^{-1} \int_V \rho_p(r)\, dV$, of the *h*-PMMA particle of volume V. Because the composite PMMA particles consist of a core of PMMA surrounded by a grafted layer of PHS, which contains an unknown quantity of solvent, we cannot determine *a priori* the solvent composition required to minimize the particle scattering. At high dilutions, the limiting coherent small-angle scattering $I(q \rightarrow 0)$ from a system of spherically symmetric particles is proportional to the volume fraction of particles, φ_c, the excess particle contrast $\Delta\rho^2 = (\overline{\rho}_P - \rho_m)^2$, and the particle volume V. To find the matchpoint, we plot $(I(q \rightarrow 0)/\varphi_c)^{1/2}$ as a function of the solvent scattering length density ρ_m. The result is shown in Figure 4a where the scattered intensity vanishes at $\rho = 0.11 \times 10^{-6}$ Å^{-2}, which is thus the average scattering length density of the PMMA particles.

For a particle consisting of a concentric core and shell, there are complications in the application of the contrast variation technique. While particle matching (choosing a solvent composition so that $\rho_m = \overline{\rho}_P$) minimizes the scattering in the $q \rightarrow 0$ limit, it does not eliminate the scattering at finite q. The strength of this nonzero q scattering depends on how different the scattering length densities (SLDs) of the core and shell of the particle are. The bigger this difference, the more inhomogeneous is the composite particle and the larger is the residual particle scattering at the matchpoint. It is important to ensure that this weak residual scattering does not, in general, exceed the scattering from the surfactant and so render the contrast variation experiment difficult to interpret.

(28) Zulauf, M.; Eicke, H. F. *J. Phys. Chem.* **1979**, *83*, 480–486.
(29) Kotlarchyk, M.; Chen, S. H.; Huang, J. S. *J. Phys. Chem.* **1982**, *86*, 3273–3276.

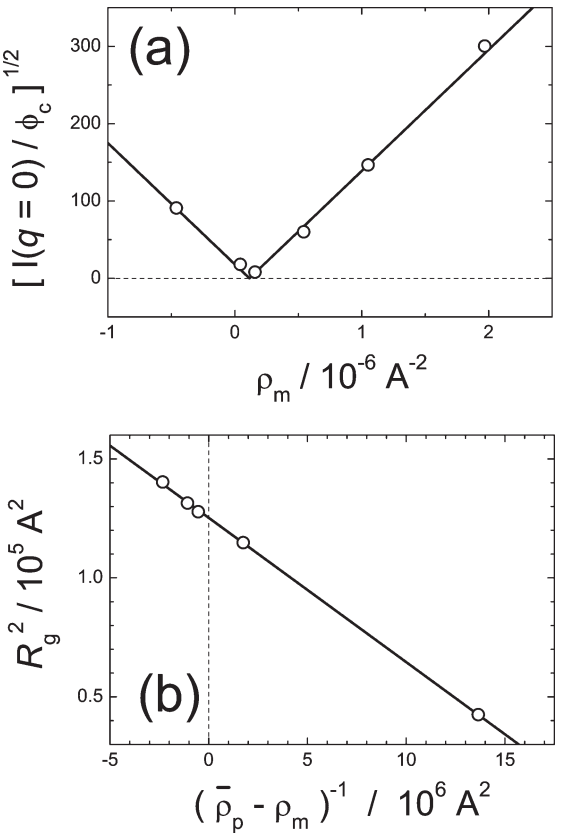

Figure 4. (a) Square root of the extrapolated intensity at $q = 0$ from nanoparticle RK2 as a function of the scattering length density of the solvent. (b) Square of the measured radius of gyration as a function of the inverse contrast, $(\bar{\rho}_p - \rho_m)^{-1}$.

To characterize the changes in the scattering length density within the particle, we determined R_g, the radius of gyration, which is defined by

$$R_g^2 = \frac{1}{(\bar{\rho}_p - \rho_m)V}\int_V r^2(\rho_p(r) - \rho_m)\,dV \qquad (13)$$

For a spherical particle consisting of two concentric layers of radii, r_a and r_b (see Figure 1), and a scattering length density profile of

$$\rho_p(r) = \begin{cases} \rho_a & \text{if} \quad r < r_a \\ \rho_b & \text{if} \quad r_a \le r \le r_b \\ 0 & \text{if} \quad r > r_b \end{cases} \qquad (14)$$

it is straightforward to derive[30,31] a simple relationship between the radius of gyration measured under different contrast conditions and the structural characteristics of the particle. A small-q expansion of eq 1 reveals that, for core−shell particles, the square of the radius of gyration R_g^2 is expected to vary linearly with the reciprocal particle contrast $(\bar{\rho}_p - \rho_m)^{-1}$, namely

$$R_g^2 = \frac{3}{5}r_b^2\left\{1 + \left(\frac{\lambda_p^2 - 1}{\lambda_p^5}\right)\frac{(\rho_b - \rho_a)}{(\bar{\rho}_p - \rho_m)}\right\} \qquad (15)$$

where $\lambda_p = r_b/r_a = 1 + \delta_p/r_a$ and δ_p is the thickness of the shell of the particle. Hence, plotting R_g^2 against $(\bar{\rho}_p - \rho_m)^{-1}$ will give a straight line with a gradient that depends on the scattering length density difference $(\rho_b - \rho_a)$ between the shell and core. The square of the radius of gyration, found by applying the Guinier approximation to the measured particle scattering in the limit $q\langle R_p\rangle \ll 1$, is plotted against the reciprocal contrast in Figure 4b using the particle matchpoint determined in Figure 4a. The line of best fit has a negative gradient signifying that the scattering length density is higher in the center of the particle than in the outer shell. The intercept with the y-axis gives the radius of gyration at infinite contrast, which from eq 15 is the R_g of a homogeneous particle of the same size r_b. The straight line through the data points cuts the y-axis at 1.25×10^5 Å^2 which equates to a geometric radius of 45.7 nm. Assuming the PHS shell has the same thickness (9 nm) as that in earlier studies,[32] we obtain for the radius of the core $r_a = 36.7$ nm and $\lambda_p = 1.25$. Substituting the linear gradient from Figure 4b and the value for λ_p into eq 15 yields a scattering length difference between shell and core, $\rho_b - \rho_a$, of -0.26×10^{-6} Å^{-2}. The relatively small difference between the contrast of the core and shell means that to a good approximation the particle scatters essentially as a homogeneous sphere, under the conditions of our experiments.

To find the individual scattering length densities of the core and shell, we use the particle match point, $\bar{\rho}_p$, which equals $(V_c/V)\rho_a + (V_L/V)\rho_b$, where V_c and V_L are the volumes, respectively, of the core and layer or equivalently $\bar{\rho}_p = \rho_b - (\rho_b - \rho_a)/\lambda_p^3$. Substitution of the experimental values found for ρ_m from Figure 4a and $\rho_b - \rho_a$ from Figure 4b yields scattering length densities of $\rho_a = 0.24 \times 10^{-6}$ Å^{-2} for the core and $\rho_b = -0.02 \times 10^{-6}$ Å^{-2} for the shell. The SLD of the shell is in good agreement with previously reported[32] values for PHS ($\rho_{PHS} = -0.06 \times 10^{-6}$ Å^{-2}) while the low value for the core in comparison to the nominal value for PMMA ($\rho_{PMMA} = 1.07 \times 10^{-6}$ Å^{-2}) supports the notion, suggested by fluorescence measurements,[33] that the particle core contains a fraction of embedded stabilizer chains. We confirmed the experimental radii were consistent with the scattering data measured over a wide q-range by performing model calculations on a system of polydisperse core−shell spheres. The values used in the model were $r_a = 36.7$ nm, $r_b = 45.7$ nm, $\rho_a = 0.24 \times 10^{-6}$ Å^{-2}, and an equivalent polydispersity of $\varepsilon_p = \langle\delta r_b^2\rangle^{1/2}/\langle r_b\rangle = 0.13$. The scattering length density of the surface layer was allowed to vary slightly around the value we determined earlier. The fits are good except in the high-q region around the second maximum of the form factor where a more complex model of the scattering length density profile within the particle, including for instance a more gradual transition from core to shell, is probably necessary to get accurate fits. Finally, the total particle radius determined by SANS $\langle R_p\rangle = 45.7$ nm is in reasonable agreement with the value found from dynamic light scattering ($R_h = 51.8$ nm), if we recognize that different techniques sample different moments of the particle size distribution. The hydrodynamic radius is the average value represented by $R_h = \langle R^6\rangle/\langle R^5\rangle$ which is related to the number average radius[34] by $R_h = \langle R_p\rangle(1 + 5\varepsilon_p^2)$. Using the polydispersity determined by SANS, the measured hydrodynamic radius equates to a mean particle radius of $\langle R_p\rangle = 47.3$ nm, which is in good agreement with the value found from SANS of 45.7 nm.

4.5. Scattering from Reversed Micelles. The size of the reversed micelles formed by d_{34}-AOT in $C_{12}H_{26}/C_{12}D_{26}$ mixtures

(30) Moonen, J.; Dekruif, C. G.; Vrij, A.; Bantle, S. *Colloid Polym. Sci.* **1988**, *266*, 836–848.
(31) Markovic, I.; Ottewill, R. H.; Cebula, D. J.; Field, I.; Marsh, J. F. *Colloid Polym. Sci.* **1984**, *262*, 648–656.
(32) Cebula, D. J.; Goodwin, J. W.; Ottewill, R. H.; Jenkin, G.; Tabony, J. *Colloid Polym. Sci.* **1983**, *261*, 555–564.
(33) Pekcan, O.; Winnik, F. M.; Egan, L.; Croucher, M. D. *Macromolecules* **1983**, *16*, 699–702.
(34) Pusey, P. N.; van Megen, W. *J. Chem. Phys.* **1984**, *80*, 3513–3520.

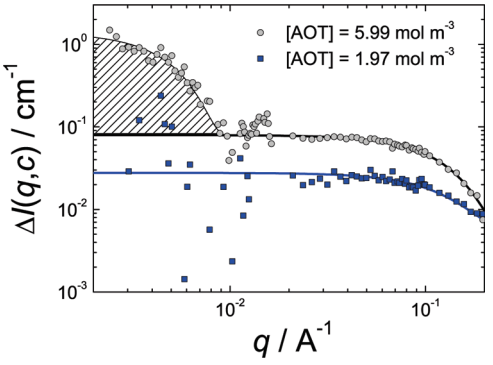

Figure 5. Difference, $\Delta I(q,c)$, between the intensity scattered by the nanoparticle/surfactant mixture and the intensity scattered by the particle without surfactant as a function of q for two different surfactant concentrations. The solid lines show the scattering expected from free micelles alone. The low-q data for [AOT] = 1.97 mol m^{-3} is noisy because the total scattering intensity is low as the particle is contrast-matched so there are large fluctuations in the calculated intensity difference.

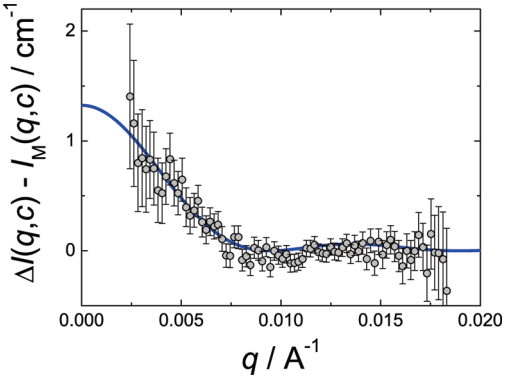

Figure 6. Excess particle scattering, $\Delta I(q,c) - I_M(q,c)$, as a function of q from a mixture of contrast-matched particles and d_{34}-AOT at a concentration of 5.99 mol m^{-3}. The solid line is a fit to the form factor given in eq 9.

was characterized by SANS (data not shown). Accurate reproductions of the scattering curves were obtained using a mean micelle radius of $\langle R_m \rangle = 1.49 \pm 0.03$ nm and a polydispersity of $\varepsilon_m = 0.12$. The measured value for $\langle R_m \rangle$ compares well with the value of 1.48 nm obtained by Kotlarchyk et al.[35] for *h*-AOT in decane.

4.6. Structure of Adsorbed Surfactant Layer. The data presented in sections 4.2 and 4.3 imply that the charge is derived from the adsorption of a surfactant species onto the surface of the particle. To identify the structure of this surface layer, we use contrast variation. First, we prepare a dilute dispersion ($\varphi_c = 0.02$) of particles in a contrast-matched solvent mixture of h_{26}-dodecane and d_{26}-dodecane. Since nothing is adsorbed on the surface of the particle, the total intensity of neutrons scattered is $I(q,0)$, in the notation introduced in section 2. The particle is contrast-matched so $I(q,0)$ is small and is dominated by the flat incoherent background. Adding deuterated AOT at a concentration c to this mixture increases the total intensity scattered as a consequence of (a) changes in the form factor of the particle as surfactant adsorbs and (b) additional scattering from reversed micelles which form to accommodate unadsorbed surfactant.[36] We identify the total coherent and incoherent scattering measured in the presence of surfactant as $I(q,c)$.

To isolate the changes in the scattering caused by the surfactant, we form the intensity difference, $\Delta I(q,c) = I(q,c) - I(q,0)$. In Figure 5, we show the q-dependent excess scattering $\Delta I(q,c)$, measured at two concentrations of added surfactant $c = 1.97$ and 5.99 mol m^{-3}. The scattering profiles were measured at contrast conditions corresponding to minimum particle scattering from Figure 4, that is, $\rho = 0.11 \times 10^{-6}$ Å^{-2}. The scattering observed at intermediate and high-q ($q > 10^{-2}$ Å^{-1}) from both samples agrees closely with the scattering expected from a dilute dispersion of reversed micelles, using the parameters determined in section 4.5. A comparison of the two concentrations however reveals a striking difference at low-q ($q < 10^{-2}$ Å^{-1}). Although there are relatively large fluctuations in $I(q)$, it is apparent from Figure 5 that the low-q scattering in the low-concentration sample is consistent with the expected micelle scattering alone. In contrast, the high-concentration sample displays a very rapid growth in the scattering at low-q (hashed in Figure 5). In this region, we are probing large length scales of order $\sim 2\pi/q$, comparable to the diameter of the particle, so that the noticeable growth in the scattering in this region indicates that, at these higher surfactant concentrations, the scattering length density profile of the particle is modified, as the surfactant adsorbs onto the particle.

To interpret quantitatively the upturn in scattering seen at low-q in Figure 5, we recall that, provided we are sufficiently close to the matchpoint of the uncoated particle so that scattering is dominated by the deuterated surfactant, we can write

$$\Delta I(q,c) = n_P \delta b_S(q)^2 + I_M(q,c) \qquad (16)$$

where δb_S is the Fourier transform of the scattering length density profile of the adsorbed surfactant $\delta\rho_S$ and I_M is the scattering from reversed micelles in solution. The micellar contribution to $\Delta I(q,c)$ is essentially constant at small-q (the solid lines in Figure 5) so subtracting this part of $I(q)$ leaves the term $n_P \delta b_S^2$, reflecting the change in the form factor of the particle as the surfactant adsorbs. This difference intensity is plotted in Figure 6 for a surfactant concentration of $c = 5.99$ mol m^{-3} and a particle concentration of $\varphi_c = 0.02$. To model this data, we assume the surfactant is adsorbed on the particle surface in a spherical band of inner radius a_s and thickness δ_s (eq 8). There is appreciable scatter in the experimental values of $\Delta I(q,c) - I_M(q,c)$, because the scattering from the adsorbed material is low, so the data is only reliable for $q \leq 0.01$ Å^{-1}, where calculations reveal that the radius a_s and the thickness δ_s cannot be identified separately from a comparison with the available data. As a compromise, we have chosen to set δ_s equal to the length of the AOT molecule (14.9 Å). The resulting fit to $n_P \delta b_S^2$, with δb_S given by eq 9, is shown by the solid line in Figure 6 for $c = 5.99$ mol m^{-3} where the low-q peak is seen to be reasonably well captured by this simple model. The interesting result is the value found for the inner radius of the surfactant layer, $a_s = 33 \pm 3$ nm, which correlates reasonably well to the core radius ($r_a = 36.7$ nm) rather than with the overall geometric radius ($r_b = 45.7$ nm) of the particle. The fitted radius a_s is insensitive to the exact value assumed for the surfactant layer thickness δ_s. Doubling δ_s to 29.8 Å, for instance, produced a fit of a comparable quality to 6 and a radius of $a_s = 32$ nm. Evidently, the AOT surfactant adsorbs on the surface of the PMMA core, deep inside the stabilizing layer rather than on to the surface of the outer PHS layer, as has been proposed in recent models.[17] For this structure to be physically realistic, there must be sufficient available space within the stabilizing layer to accommodate AOT molecules.

(35) Kotlarchyk, M.; Huang, J. S.; Chen, S. H. *J. Phys. Chem.* **1985**, *89*, 4382–4386.

(36) The contribution to the scattering from unassociated surfactant molecules in solution is assumed negligible, since the cmc is so small.

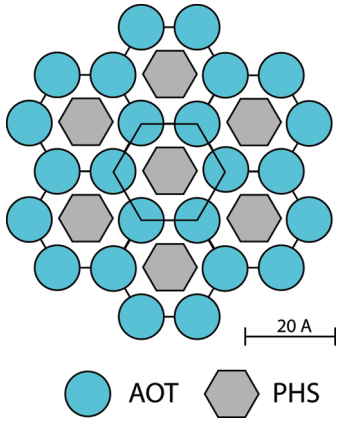

Figure 7. Schematic representation of the proposed packing of surfactant and polymer molecules at the surface of the particle. The large central hexagon has an area of 400 Å^2 and denotes the estimated area per PHS chain.

While we do not know the surface density of the stabilizing chains used in our experiments, Hill[32,37] has estimated from stability and radio-labeling studies that stable PMMA particles require a minimum packing of approximately 400 Å^2 per chain. Particles with areas per chain larger than 400 Å^2 were observed to be colloidally unstable. Since the area occupied by one PHS chain in a hexagonally packed array is only about 94 Å^2, we expect that while the conformations of PHS chains will be constrained by their neighbors,[38] there is still substantial space in the layer, as much as ~300 Å^2 of surface available per chain. The maximum cross-sectional area of the polar sulfonated headgroup of the AOT molecule is about 55 Å^2, and the molecule is about 11 Å long.[39] However, there is strong evidence[35,40] that a hydrogen-bonded network consisting of a tightly bound layer of water and the sodium counterion with a thickness of 4−5 Å develops around the polar headgroup so that the effective surfactant length is probably nearer to 15 Å. Assuming, for simplicity, that the PHS chains are hexagonally packed on the surface of the particle, we sketch in Figure 7 a plausible arrangement of the AOT molecules within the stabilizing layer. The radius of the largest species which can just fit between three neighboring PHS chains is about 6.5 Å, so while there is insufficient space within the layer to accommodate a micelle (R_m = 14.9 Å), there is plenty of room for a vertically aligned AOT molecule (shown by the blue circles in Figure 7). While the actual molecular packing at the particle surface is probably more disordered than the idealized structure sketched in Figure 7, this arrangement does account for the anomalously high limiting surface area per AOT molecule found by adsorption. Assuming all available sites are occupied by AOT molecules, there would be two AOT molecules per PHS chain, and accordingly, we would expect an area per AOT chain of about 200 Å^2, which is broadly in line with the experimentally determined value of Γ = 260 Å^2. We conclude, therefore, that there is sufficient room within the stabilizing layer to accommodate individual AOT molecules, but not micelles.

4.7. Charging Mechanism. The structural evidence presented in section 4.6 suggests that nonpolar PMMA particles probably charge via a two-step process: AOT molecules first adsorb into the stabilizing layer around each particle and then ionize, generating a surface-bound surfactant ion and a mobile counterion. This ion is stabilized by being encapsulated inside one of the large number of reversed micelles in solution. We now examine this mechanism in detail and in particular analyze whether this process is quantitatively consistent with the dependence of the surface potential on the concentration of added surfactant, displayed in Figure 2b. Our model is a straightforward extension of that originally proposed by Hsu et al.[10,12] but one in which we explicitly allow for both adsorption and dissociation, rather than assuming the particle charge is generated by the ionization of a fixed number of chemically bound surface groups. We assume that our particles are completely apolar and have no chemically bound surface charges. They charge only as a result of surfactant adsorption. For clarity, we summarize the main features here but for explicit details we refer the reader to previous theoretical work.[10,12,17]

If a nonpolar particle is to charge in equilibrium, surfactant molecules must adsorb onto the surface and dissociate and the resulting ions must be separated by a distance comparable to the Bjerrum length λ_B to prevent recombination. Both processes, ionization and counterion separation, lead to a gain in entropy, and if charging is to be spontaneous, the total increase in entropy must offset the energetic cost of ion generation and separation. If a particle has a total of N surface sites for surfactant adsorption, Σ of which are occupied by surfactant molecules of which Z are ionized, then the increase in the surface entropy as the number of ionized molecules is increased to $Z + 1$ is $dS_s/dZ = k_B \ln((N - \Sigma)/Z)$. Ionization of an adsorbed surfactant molecule also contributes a bulk entropic term as the Z counterions are distributed among the reversed micelles in solution. If the number of micelles per particle is M, then the increase in the ideal entropy of mixing per unit charge in the bulk is $dS_b/dZ = k_B \ln((M - Z)/Z)$. At equilibrium, the reduction in the free energy due to these two favorable entropic processes must exactly balance the energy required to create the ions and to separate the counterions from the electrostatic field of the charged particle. If the energy (in units of k_BT) to create a surface-bound surfactant ion is g_s, g_b is the self-energy of the counterion, and $\psi = e\varphi/k_BT$ is the energy cost to separate the counterion from the particle, then at equilibrium

$$g_s + g_b + \Psi + \ln(Z/(N - \Sigma)) + \ln(Z/(M - Z)) = 0 \qquad (17)$$

This equation may be solved if we recognize that, provided the surface potential is sufficiently low and $\kappa R_p < 1$,[41] the particle charge Z may be replaced by the expression $Z = R_p\psi/\lambda_B$ and the equation closed. Evaluating the equilibrium condition (eq 17) at two different surfactant concentrations, c_1 and c_2, and subtracting the expressions yields a simple algebraic condition on the equilibrium surface potential measured under different conditions, namely

$$\Psi_2 \, e^{(1/2)\Psi_2} = \sqrt{K}\Psi_1 \, e^{(1/2)\Psi_1} \qquad (18)$$

where Ψ_i (i = 1,2) are the surface potentials measured at the concentrations c_i and K is the density-dependent ratio, $K = [c_2(N - \Sigma_2)]/[c_1(N - \Sigma_1)]$. If, furthermore, we assume the adsorption of surfactant onto the surface of the particle is described by a Langmuir isotherm, $\Sigma = N\alpha c/(1 + \alpha c)$, where α is the Langmuir adsorption constant, then the ratio K may be written as $K = [c_2(1 + \alpha c_1)]/[c_1(1 + \alpha c_2)]$. The concentration dependence of the surface

(37) Hill, R. Ph.D. Thesis, University of Bristol, Bristol, **1981**.
(38) The constraints on available chain conformations are more marked because the PHS chain is branched. As a consequence, the PHS chains are likely to be fully extended away from the surface.
(39) De, T. K.; Maitra, A. *Adv. Colloid Interface Sci.* **1995**, *59*, 95–193.
(40) Wootton, A.; Picavez, F.; Harrowell, P. *AIP Conf. Proc.* **2008**, *982*, 289–294.
(41) The data in Figure 2a show that this is a reasonable assumption except at the highest surfactant concentrations.

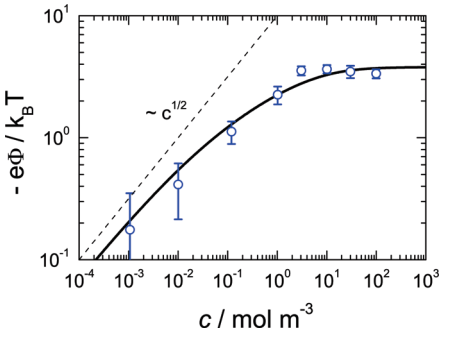

Figure 8. Surface potential as a function of surfactant concentration. Experimental data are plotted as open symbols, and the fit to eq 19 is shown as the solid line.

potential $\psi(c)$ follows directly from the formal solution of eq 18 in terms of the Lambert $W(z)$ function,[42]

$$\Psi(c) = 2W\left(\frac{1}{2}\Psi_1 \, e^{(1/2)\Psi_1} \, K^{1/2}\right) \tag{19}$$

where Ψ_1 is the surface potential measured at a surfactant concentration of c_1 and $K = [c(1 + \alpha c_1)]/[c_1(1 + \alpha c)]$. Inspection of eq 19 reveals that the potential Ψ initially grows with increasing surfactant concentrations, since, in the limit of small c, K is proportional to the concentration. The developing charge on the particle however suppresses the dissociation of the adsorbed AOT molecules so the potential grows more slowly than the square-root dependence, $\Psi \propto c^{1/2}$, expected for the dissociation of surfactant monomers. In this limit, eq 19 is identical to the model proposed by Sainis et al.[10] The crucial difference in our work is the inclusion of both adsorption and dissociation processes so that, in the limit of high surfactant concentration, K becomes independent of c and consequently the surface potential Ψ saturates, as all the surface sites on the particle become occupied by surfactant molecules. Using the value of Ψ at $c = 1$ mol m^{-3} as a reference, we vary the value of α and calculate the surface potential Ψ as a function of the surfactant concentration. The results of this calculation for $\alpha = 0.08$ mol^{-1} m^3 are plotted as the solid line in Figure 8 together with the measured surface potentials, presented in section 4.2. The calculated values are in near quantitative agreement with the values obtained from experiment and provide further support for the mechanism of adsorption and dissociation. The only parameter in this comparison is α, proportional to the binding energy of adsorption, which controls the maximum surface plateau and the surfactant concentration at which the surface potential saturates.

The model also predicts that the saturated surface potential at high surfactant concentrations should be independent of the particle size, consistent with the observations detailed in section 4.2. To see this, we rewrite eq 17 as

$$\Psi^* + 2\ln \Psi^* = \ln C - (g_s + g_b) \tag{20}$$

where $\Psi^* = \lim_{c\to\infty} \Psi(c)$ and $C = (N - \Sigma)M\lambda_B{}^2/R_p{}^2$. Assuming Langmuir adsorption, the number of free sites $N - \Sigma$ is $N/(\alpha c)$, which is proportional to $R_p{}^2$ since the total number N of surface sites is $4\pi R_p{}^2/A$, where A is the limiting area per surfactant molecule. The number of micelles per particle, M, is $cN_A/(N_{as}n_P)$ where N_A is Avogadros's constant, N_{as} is the micelle association number, and n_P is the particle number density. In this case, C reduces to the size-independent constant

$$C = \frac{4\pi\lambda_B{}^2 N_A}{A\alpha N_{as} n_P} \tag{21}$$

The solution of eq 20 can be written as

$$\Psi^* = 2W\left(\frac{1}{2}C^{1/2} \, e^{-[(1/2)(g_s+g_b)]}\right) \tag{22}$$

Therefore, in the high concentration limit, the surface potential is governed by the free energies of ion formation and is independent of particle size. Taking $\Psi^* = 3.5$, $A = 260$ Å^2, $\alpha = 0.08$ mol^{-1} m^3, $N_{as} = 28$, and $n_P = 10^{13}$ m^{-3} (equivalent to a volume fraction of 10^{-5} for the 425 nm particles), we calculate, from eq 22, $g_s + g_b = 25.2k_BT$. Combining this value with the known free-energy cost of ionizing a single isolated micelle[17] ($g_b = 11.8k_BT$), we estimate that the energy cost of charging the ion on the particle surface is $g_s = 13.4k_BT$. The observation that $g_s > g_b$ is consistent with the model of the surface structure obtained from SANS (see Figure 7), since isolated AOT molecules are unlikely to be able to solvate charges as effectively as micelles in solution.

5. Conclusions

The mechanism by which surfactants generate particle charging in low polarity solvents has been examined using a combination of single particle microelectrophoresis, adsorption studies, and small-angle neutron scattering. Using a model system, consisting of polymer-grafted poly(methyl methacrylate) nanoparticles and the well characterized surfactant, AOT, in *n*-dodecane, we have shown that particle charging in nonpolar solvents is qualitatively different from that observed in aqueous solvents. Particles, with no chemically bound surface groups, charge by adsorption of surfactant molecules, a small fraction of which ionize with the liberated counterions becoming solubilized in reversed micelles. The subsequent buildup of charge on the surface of the particle suppresses the expected square-root concentration dependence of the ionization of adsorbed species so that the surface potential of the particle is a rather gradual function of the surfactant concentration, $\Phi \sim c^{0.4}$. At high surfactant concentrations, the surface potential saturates to a value which is controlled by the maximum level of surfactant adsorption achieved.

Acknowledgment. The authors thank Dr. Bruno Demé for his help as the local contact on D11 and the Institute Laue Langevin, Grenoble for the generous provision of neutron beam time. We also thank the Oxford Isotope Facility for the supply of deuterated 2-ethyl hexanol. R.S. and R.K. acknowledge financial support from the University of Bristol Overseas Research Scheme and the Engineering and Physical Sciences Research Council.

(42) Jean-Michel, C. *J. Phys. A* **2003**, *36*, 10431.